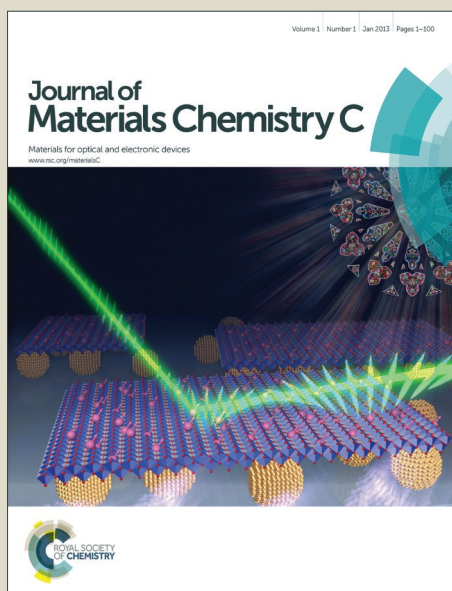


Journal of Materials Chemistry C

Accepted Manuscript



This is an *Accepted Manuscript*, which has been through the Royal Society of Chemistry peer review process and has been accepted for publication.

Accepted Manuscripts are published online shortly after acceptance, before technical editing, formatting and proof reading. Using this free service, authors can make their results available to the community, in citable form, before we publish the edited article. We will replace this *Accepted Manuscript* with the edited and formatted *Advance Article* as soon as it is available.

You can find more information about *Accepted Manuscripts* in the [Information for Authors](#).

Please note that technical editing may introduce minor changes to the text and/or graphics, which may alter content. The journal's standard [Terms & Conditions](#) and the [Ethical guidelines](#) still apply. In no event shall the Royal Society of Chemistry be held responsible for any errors or omissions in this *Accepted Manuscript* or any consequences arising from the use of any information it contains.

A broadband bidirectional visible light absorber with wide angular toleranceLei Zhou, ^{*a} Yun Zhou, ^b Yu-Fu Zhu, ^c Xiao-Xuan Dong, ^b Ben-Ling Gao, ^aYan-Zong Wang, ^a Su Shen ^{*b}

^a Faculty of Mathematics and Physics
Huaiyin Institute of Technology
Huai'an 223003, PR China
E-mail: zhzhlei@gmail.com (Dr. L. Zhou)

^b College of Physics Optoelectronics and Energy
Soochow University
Suzhou 215006, PR China
E-mail: shen.su@gmail.com (Dr. S. Shen)

^c Faculty of Mechanical Engineering
Huaiyin Institute of Technology
Huai'an 223003, PR China

† Electronic Supplementary Information (ESI) available.

Keywords:

light absorber, bidirectional, quasi-periodic, nanocone array, visible light

Abstract

Along with significant efforts devoted to the development of high-performance light absorber architectures, impressive results have already been achieved for coupling photons to conduction electrons. Nevertheless, the energy harvesting is limited as the previously reported light absorbers could only absorb the light from one incident direction. In the present work, we developed for the first time a wide-band bidirectional visible light absorber (BLA) based on quasi-periodic nanocone array coated with a dielectric-loaded mono-layer of gold. Clearly unlike conventional light absorbers, our proposed BLA is capable of absorbing light from front surface and rear surface simultaneously, yielding measured average front absorption of 87.4% and the corresponding 76.2% rear absorptivity from 300 nm to 700 nm, respectively. Moreover, the bidirectional absorption property retains well with respect to the incident angle varying from 0° to 60°. The experimental and theoretical analyses indicate that these interesting absorption properties can be ascribed to the combination of the localized cavity resonant mode (CM), the localized surface plasmonic mode (SPM), the guided-mode resonance (GMR) and the hybrid coupling between CM and SPM. We anticipate that our concept provides a new pathway for fabrication of large-area new types of flexible or wearable solar thermoelectrics, photodectors or other solid-state devices.

1. Introduction

Since Landy *et al.* proposed a single-wavelength perfect absorber in 2008,¹ light absorbers have been gaining increasing importance in sunlight-harvesting applications

such as thermophotovoltaic cells,² sensor detection,³ biomedical imaging,⁴ photon detection⁵ and nanostructure-assisted ionizations and ablation.⁶⁻⁷ To date, various light energy absorber configurations and materials have been extensively demonstrated to increase the absorption from gigahertz and terahertz regimes to visible frequencies,⁸⁻⁹ Such as metal-insulator-metal (MIM) cavity,¹⁰⁻¹¹ metamaterial-based surfaces,¹²⁻¹³ metallic nanostructures,¹⁴⁻¹⁵ black silicons,¹⁶ nanowires¹⁷⁻¹⁸ and so on.¹⁹⁻²⁰ To fulfill the fundamental demanding requirements of harvesting more photons, new device architectures have usually been designed for pursuit of wavelength-, angle-, and polarization-independence.²¹⁻²² Some new device architectures have been proposed to broaden the absorption band. For example, Yang *et.al* theoretically designed an ultra-broadband absorber based on metallic nanogrooves of different depth.²³ Narimanov *et.al* have suggested an optical black holes capable of absorbing electronic and magnetic over a large frequency range based on transformation optics design method.²⁴ Nevertheless, these design concepts contain the miniature and elaborate structures parameters like 10 nm width and 5 μm depth, which is almost impossible to be straightforwardly realized by current fabrication technologies. To overcome these bottlenecks, various device geometries have been further exploited, For example, Sondergaard *et al* proposed a broadband absorber consisting of two-dimensional array of sharp convex grooves, yielding > 87% absorption over 450-850 nm,²⁵ while Giulia Taglia bue *et al* realized an ultrabroadband, wide angle and polarization-insensitive light absorber (88% average absorption in the range of 380-900 nm) featuring tapered triangle nanopatterning films.²⁶ Mihail Bora *et al* developed a plasmonic resonant

visible light absorber composed of a square array of vertically coupled nanowires coated with metal film, achieving ~75% average absorption over the visible range of 400-800 nm despite wavelength dependence.²¹ Mehdi, K. H *et al* and Hedayati, M. K *et al* proposed perfect plasmonic metamaterial absorbers with amazing absorption around 100% in the entire visible region, respectively.²⁷⁻²⁸ Although impressive results have already been achieved for coupling photons to conduction electrons due to the significant efforts devoted to the development of high-performance light absorber architectures, so far the reported conventional concepts have only focused on absorbing the light from one incident direction, which inevitably limits their utility for energy harvesting. Herein, design considerations for optimal structures aiming at absorbing light from both front and the rear incident surfaces simultaneously are urgently required for enhancement in the energy harvesting of light absorbers.

Here, we present the design, fabrication, and characteristics of a novel wide-band bidirectional visible light absorber (hereafter termed BLA) based on quasi-periodic nanocone array coated with a dielectric-loaded mono-layer of gold. Clearly unlike common light absorber, our proposed BLA is capable of absorbing light from the front surface and rear surface simultaneously, yielding measured average absorption of 87.4% when light is incident on the front surface and corresponding 76.2% while incident light illuminated rear surface from 300 nm to 700 nm, respectively, where the full absorption width at a half maximum (FWHM) are about ~100% and ~86.1%, respectively. Moreover, the bidirectional absorption property retains well with respect to the incident angle varying from 0° to 60°. The experimental and theoretical

analyses indicate that these interesting absorption properties can be ascribed to the combination of the localized cavity resonant mode (CM), the localized surface plasmonic mode (SPM), the guided-mode resonance (GMR) and the hybrid coupling between CM and SPM. The proposed method is quite simple, cost-effective and compatible with low temperature plastic substrates, which makes it potential application in thermo photovoltaic cells, thermal emitters and other light trapping optoelectronics.

2. Experimental

2.1. Fabrication Procedure. Fig. 1 schematically illustrates the fabrication process of BLA by two-step anodization process followed by soft nanoimprinting lithography (SNIL) and RF magnetron sputtering. First, an anodized aluminum oxide (AAO) mother-template was fabricated by two-step anodization process.²⁹ As shown in Fig. 1a-b, high pure aluminum foil (99.999% purity, 0.25 mm thickness) was cleaned in acetone and isopropyl alcohol in sequence. After that, the aluminum foil was immersed in oxalic acid (0.3 M) with a constant-voltage of 40 V and the solution temperature was kept at 5° for 4 h. During which time, the solution was stirred by a pump circulation system. Then, the second anodization process is processed under the same conditions as the first anodization step for 6 min. Subsequently, the AAO foil was etched in phosphoric acid solution (6 wt%) at 32° for 10 min to remove the anodic aluminum oxide layer and wider the pore diameter. As a consequence, the aluminum foil with controlled pore size was cleaned with deionized-water and thus

the AAO mother-template was obtained. To fabricate the quasi-periodic nanocone array, the UV-resin (D10, PhiChem) was drop-casting onto the pre-fabricated AAO mother-template with thickness of $\sim 1 \mu\text{m}$ (Fig. 1c). Then, plastic PET substrate was put closely upon the drop-casted UV resin and imprinted under a constant pressure 1.5 bar for 15 s with UV illumination at light power intensity of 500 mJ cm^{-2} at a wavelength of 395 nm, and the quasi-periodic nanocone array constructed on PET substrate were obtained after peeling off the AAO template carefully (Fig. 1d). Finally, the well-designed 20 nm-thick Au mono-layer and 18 nm-thick Si_3N_4 layer (cf. ESI S1 & S2) were subsequently deposited on the UV nanocone array by RF magnetron sputtering³⁰⁻³¹ and thus the proposed BLA was obtained successfully.

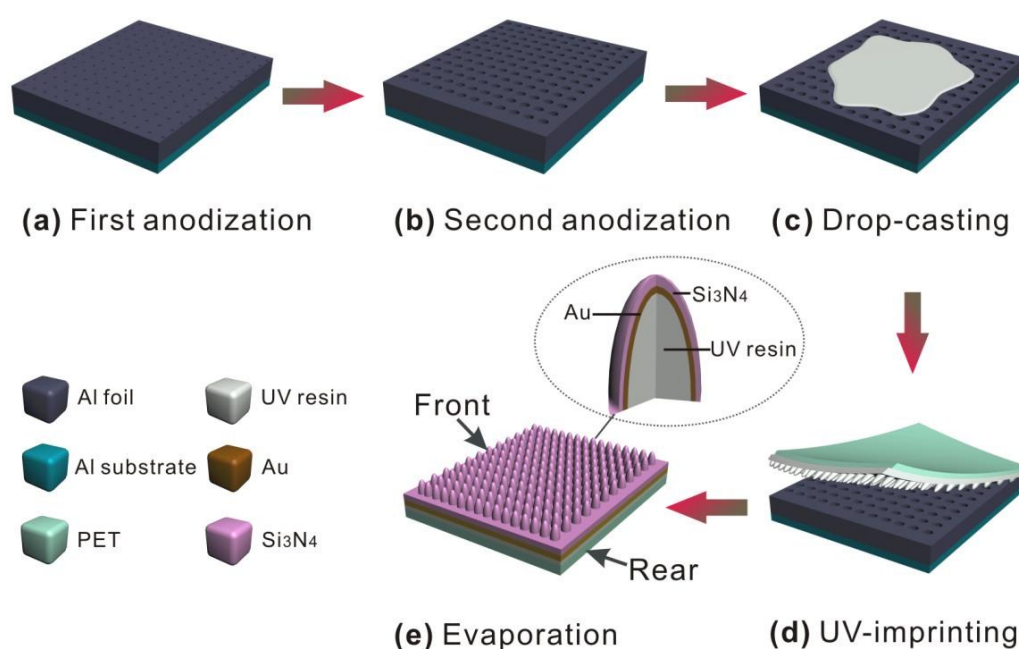


Fig. 1 Schematic of the fabrication process of the bidirectional visible light absorber.

(a) The first anodization process. (b) The second anodization process. (c)

Drop-casting UV resin on glass substrate. (d) Imprinting UV resin by UV-assisted nanoimprinting lithography followed by demolding process. (e) Depositing the Au layer and Si₃N₄ layer onto the quasi-periodic nanocone array with thickness of 20 nm and 18 nm, respectively.

2.2. Properties Characterizations. The thickness, refractive index (n), extinction coefficient (k) and film thickness of all the layers were measured using the alpha-SE™ Spectroscopic Ellipsometer (J. A. Woollam Co., Inc). Optical transmission spectra were recorded by a UV/vis/near-IR spectrophotometer (Perkin Elmer Lambda 750) with an integrating sphere. Surface morphologies were characterized by AFM (Veeco MultiMode V) in tapping mode and SEM (FE-SEM, Quanta 400 FEG).

2.3. Optical Simulation: To find a rigorous solution to Maxwell's equations in the flat and BLA samples, the three dimensional finite difference time domain (FDTD) method was adopted to calculate a the optical near-field behaviors, the spectral response and Poynting vector \mathbf{S} distributions (RSoft Full Wave and corresponding codes generated in house using Matlab software) with commercial RSoft 8.1 (RSoft Design Group, Inc), where the quasi-periodic nanocone array were arranged in the range of ~ 10 periods, based on morphologies obtained from SEM and AFM measurements. Nonuniform grid was set to model different parts of the samples in order to accelerate precise calculation quickly with efficient usage of memory. The complex optical dielectric function of the Au cathode was fitted using Drude-Lorentz

model, taking into account interband transitions and the wavelength-dependent n and k values of the other dielectric constants experimentally determined by the ellipsometric measurements.

3. Results and discussion

3.1. Device Structure. The structural features of the AAO mother-template and UV nanocone array constructed on PET substrate were characterized by scanning electron microscopy (SEM), and presented in Fig. 2a, b respectively. It can be clearly seen that the structure of AAO membrane exhibits densely array of columnar cells and the duplicated UV nanocone array displays approximately parabolic topography with a period of ≈ 180 nm, fill factor of ≈ 0.35 and groove depth of ≈ 300 nm, indicating that morphology of UV nanocone array is exactly complementary for AAO template and the high-fidelity replication results are in accordance with our previously demonstration.³²⁻³⁴ Fig. 2c, d display atomic force microscopy (AFM) images of 20 nm-thick mono-layer Au deposited on UV nanocone array and 18 nm-thick Si_3N_4 deposited on Au layer, respectively. Tapping-mode AFM characterizations of these images reveal that nanostructured Au layer presents a period of ≈ 180 nm, fill factor of ≈ 0.5 , groove depth of ≈ 290 nm and the surface root-mean-square (RMS) roughness of 9.56 ± 0.06 nm, while Si_3N_4 layer subsequently coated on Au layer displays a period of ≈ 180 nm, fill factor of ≈ 0.7 , groove depth of ≈ 270 nm and RMS roughness of 6.73 ± 0.04 nm, respectively. The uniform corrugated morphology of Si_3N_4 confirms the conformal coating of Au layer on the quasi-periodic UV-resin

nanocone array. Notably, the approach proposed here capitalizes on the scalability and high throughput of roll-to-plane and roll-to-roll SNIL technique and, thus, enables fabrication of large-area new types of flexible or wearable thermophotovoltaics, photodectors or other solar thermoelectrics.

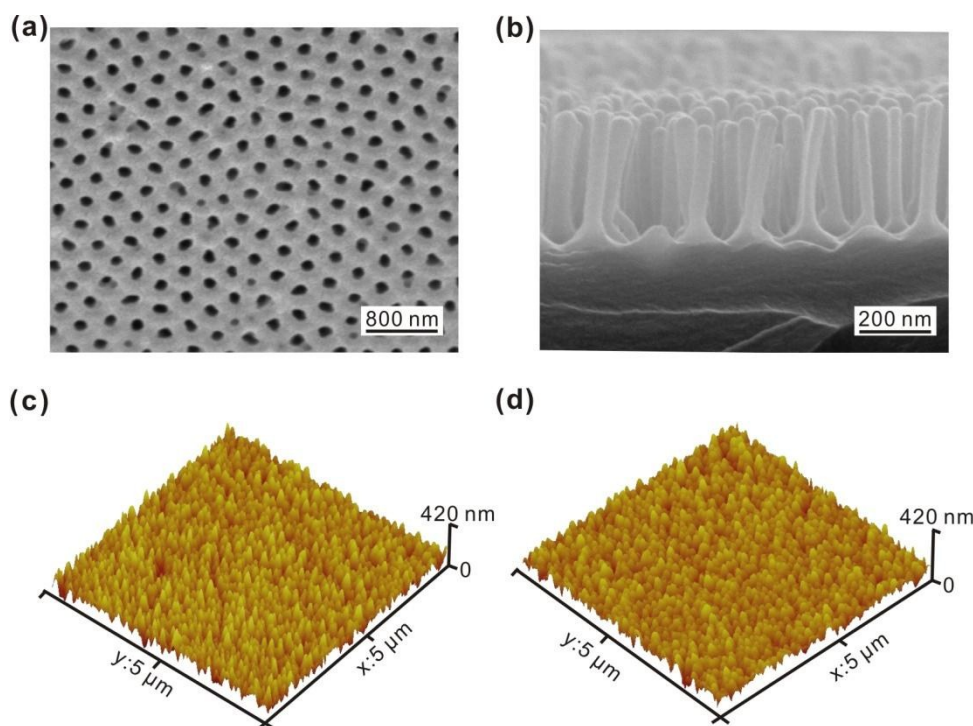


Fig. 2 Device morphologies characterization. SEM images of (a) AAO template with a quasi-periodic pore array, (b) cross-section UV nanocone array (period: ≈ 180 nm, groove depth: ≈ 300 nm, fill factor: ≈ 0.4). AFM images of (c) mono-layer Au deposited on the UV nanocone array constructed on PET substrate with thickness of 20 nm, (d) Si_3N_4 layer deposited on the Au layer with thickness of 18 nm.

3.2. Light absorption properties. To clearly shedding light onto the absorption capability of the BLA, flat devices with a configuration of PET/UV-resin film (1

μm)/Au layer (20 nm)/ Si_3N_4 (18 nm) are also fabricated for comparison. Bidirectional total transmission (T), reflection (R) and absorption (A) from a flat and a BLA are measured and performed in Fig. 3a-d, respectively. As apparently displayed in Fig. 3a, the front absorptivity of the flat absorber decay dramatically from 300 nm to 800 nm in the entire visible regime with maximum absorption is as low as 63.4% (@ 300 nm), resulting in corresponding high average transmission (56.3%) and reflection (16.3%). Additionally, although the rear transmission and rear reflection profiles are slightly different from that of the front when the incident light radiates on the rear surface, the rear absorptivity display a similar spectra (Fig. 3b), which is attributed to the different optical refractive indexes of the front ($n_{\text{Si}_3\text{N}_4} = 2.5$) and the rear dielectric ($n_{\text{PET}} = 1.46$). These results clearly reveal that there are lots of light can propagation through such a thin flat structure, implying relatively poor capabilities in light harvesting and conversion. In comparison, the optical properties of the proposed BLA were characterized. According to the measured results in Fig. 3c&d, it is easy to find that the BLA exhibits an ultra-broad absorbing band, yielding measured average front absorption of 87.4% and corresponding rear absorption of 76.2% from 300 nm to 700 nm, respectively, where the full absorption width at a half maximum (FWHM) are about ~100% and ~86.1%, respectively (Fig. 3c&d). Furthermore, it is noteworthy that the front absorptivity in the experiments are generally lower than the calculated data (cf. ESI S2), which could be attributed to additional scattered light induced by the experimental surface roughness.³⁵ In addition, to further probe the capabilities of the BLA, the angle-dependent absorption spectra for two independently incident

direction are tested and presented in Fig. 3e,f, respectively. It is seen that the absorption curves appear slightly variation as function of wavelength, but the bidirectional absorption property retains well with respect to the incident angle varying from 0° to 60° , resembling that of at normal incidence as shown in Fig. 3c&d. These significant experimental results distinctly demonstrate that the proposed structure possesses bidirectional robust angle-tolerance and opens up new opportunities to develop and optimize thermoelectric architectures for omnidirectional light harvesting. As a result, the visualized flat sample and BLA under the fluorescent lamp irradiation and the ambient light corresponding to their bidirectional structural features are presented in Fig. 4a-d. A significant feature directly observed from these photographs is that the BLA provides bidirectional broadband efficient light harvesting and results in a nearly black image, while the flat samples display a vivid semi-transparent image, which clearly indicates that a large portion of the bidirectional incident photons are reflected or transmit the flat architecture. Obviously, these noticeable results correspond very well to the measured data as shown in Fig. 3.

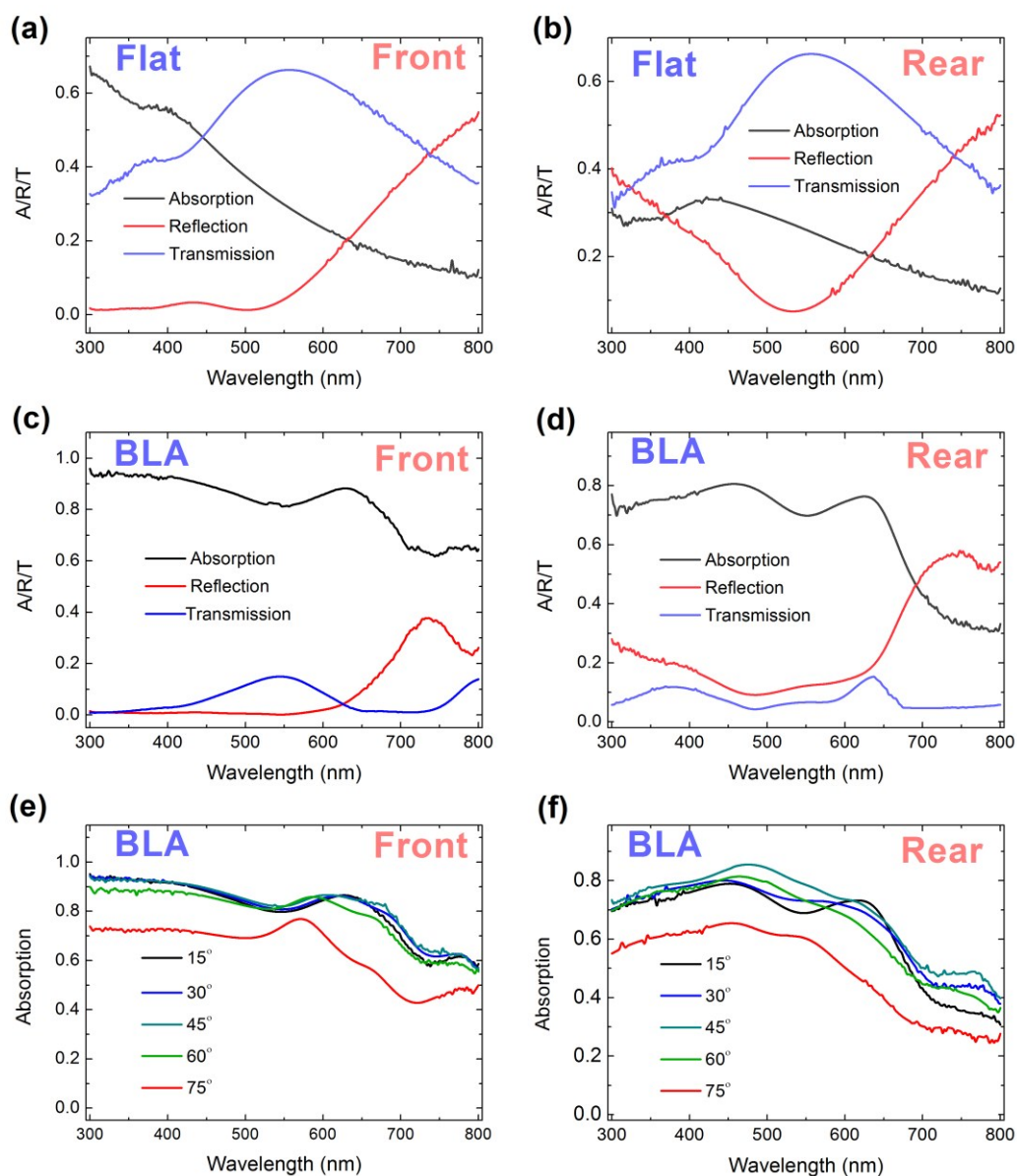


Fig. 3 The measured bidirectional optical properties for the samples in the direction normal to the PET substrate. A/R/T spectra of a flat absorber with incident light radiate on (a) the front surface and (b) the rear surface. A/R/T spectra of a BLA with light radiate on (c) the front surface and (d) the rear surface. The measured angle-dependent absorption spectra of a BLA from 30° to 75° in 15° steps with the incident light illuminate (e) the front surface and (f) the rear surface.

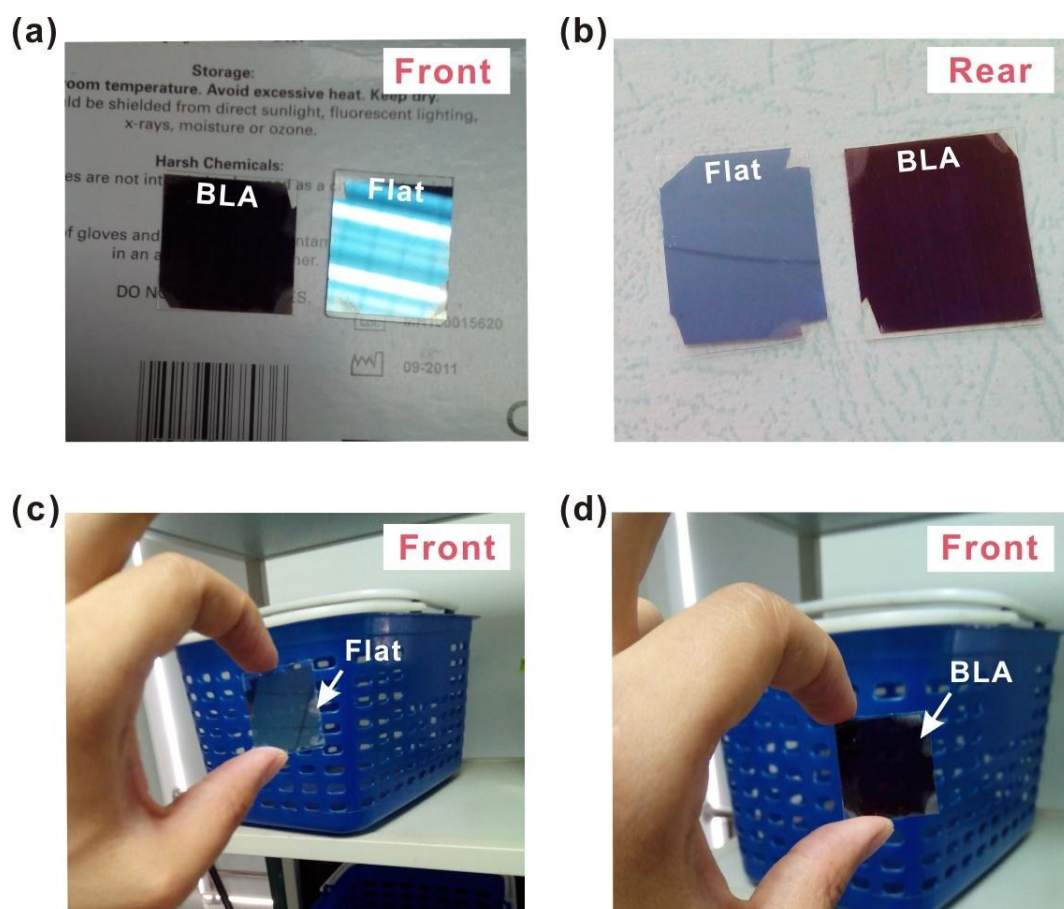


Fig. 4 Photography of flat and proposed BLA with the size of $2.5 \times 2.5 \text{ cm}^2$ under (a) fluorescent lamp irradiation towards the front surface and (b) a daylight-lit room environment illuminated the rear surface. Photography of (c) flat and (d) proposed BLA placed on the front of a common basket under the ambient light with the size of $2.5 \times 2.5 \text{ cm}^2$, respectively.

3.3. Optical simulation. To analyze and understand the observed broadband high absorption capabilities of the BLA, the three-dimensional finite-difference time-domain (FDTD) method was adopted to calculate the optical near-field

behaviors, the spectral response and Poynting vector distributions. The magnetic field intensities at the resonant wavelength of 540 nm and 620 nm observed in Fig. 3 for BLA were simulated and displayed in Fig. 5. The field “behind” the interface of air/Si₃N₄ is very smaller than that of corresponding flat architecture when incident radiates on the front surface in normal direction (Fig. 5a & ESI S3), implying the zero order reflection is strongly suppressed. The reason is ascribed to localized cavity resonant mode (CM) associated with surface plasmonic mode (SPM) excited around the dielectric/metal composite nanostructured interfaces, which gives rise to omnidirectional absorption.³⁶⁻³⁷ Meanwhile, note that the field “above” the PET substrate is slightly larger, demonstrating that a small portion of photons could escape from the device resulting in the corresponding dip of the absorption (@540 nm), which is attributed to Rayleigh-Wood anomalies.³⁸⁻³⁹ This fact is perfectly consistent with the A/R/T characteristics observed in Fig. 3c. For comparison, the corresponding magnetic field intensity (@540 nm) for rear illumination was also calculated (Fig. 5b). It can be observed that the field intensity “behind” the interface of PET/Au is obviously larger than that of front illumination, suggesting a larger reflectivity and thus lower absorbtivity, which is attributed to an abrupt change in refractive index at the PET/Au interface. Thereby, the absorption at 540 nm is mainly due to the localized CM and localized SPM, and the visualized absorbtivity decreasing induced by Rayleigh-Wood anomalies. To unveil the physical origins behind the resonant peak at 620 nm, the bidirectional magnetic field intensity distributions were also calculated. As shown in Fig. 5c, d, it is clear that the magnetic field is strongly localized in the

Au/Si₃N₄ region around the top and bottom, revealing that the contributions for this absorbtivity peak could be provided by the similar localized CM and localized SPM effects. Interestingly and importantly, the strong confined sub-centre field is observed in the areas close to the middle of the UV-nanonipples, which corresponds to the guided-mode resonance (GMR) induced by the electromagnetic interference of the incident wave with the scattered evanescent field.⁴⁰ Besides, compared with the front absorption field profile discussed above, the rear absorption field “above” the air line (Fig. 5d) was increased slightly, indicating relatively higher transmittance, which is in good agreement with the experimental measurement as discussed above (Fig. 3c&d). Therefore, the absorption at 620 nm is mainly due to the localized CM, localized SPM, and GMR. To better reveal the angle-robust absorption capability of the BLA, the angular evolution of magnetic field intensity distributions excited by a TM polarized plane were also performed (cf. ESI S4). Remarkably, the intensities of the field beyond the incident interfaces when the incident angle increase to 60° is still as low as that of in the direction normal, showing a reasonable agreement with the tested curves depicted in Figure 3e, f. These calculation results provide directly theoretical support that localized CM plays the key role in this case, because of field is strongly localized around the metallic corners. However, according to the classic CM resonant theory and the SPM excitation equation $k_{sp} = k_{inc} \pm mG$ ($m = 0, 1, 2, \dots$), respectively, both of these modes are sensitive to incident angle in nature,⁴¹⁻⁴² therefore, it can be inferred that the hybrid interference between SPM and localized CM must be occurred when oblique light incident.

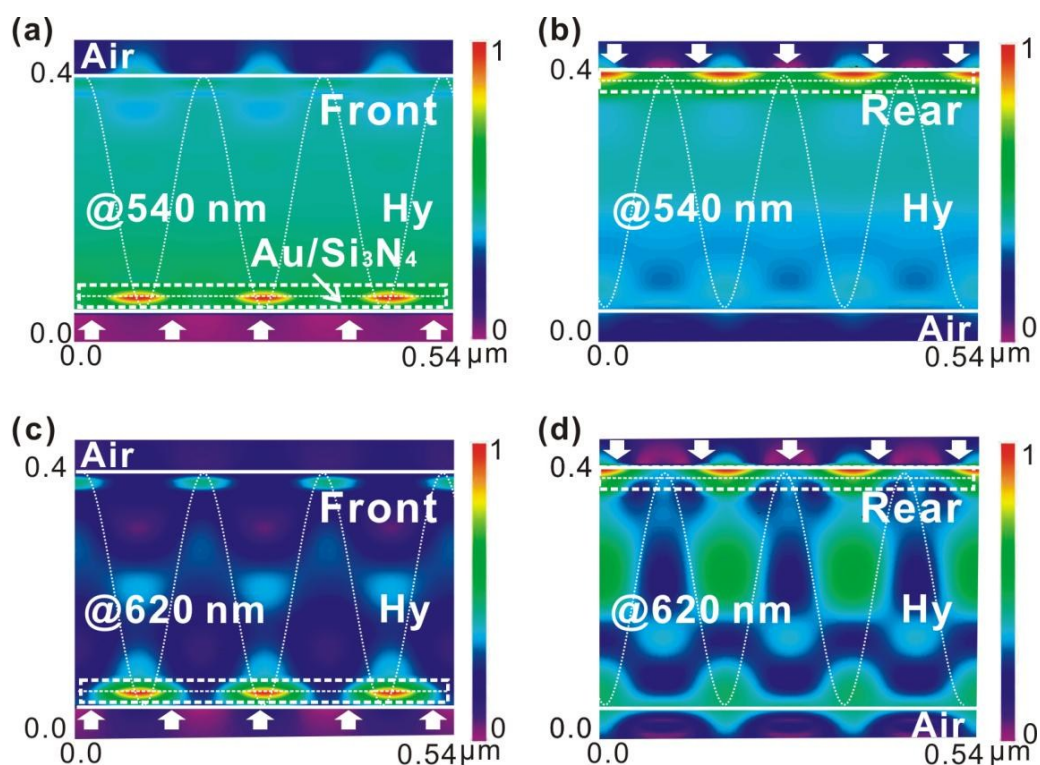


Fig. 5 Calculated normalized near-field distributions of the magnetic field intensity excited by a TM polarized plane wave for BLA at a wavelength of (a) 540 nm (front), (b) 540 nm (rear), (c) 640 nm (front) and (d) 640 nm (rear), respectively. The white lines denote the interface of different materials.

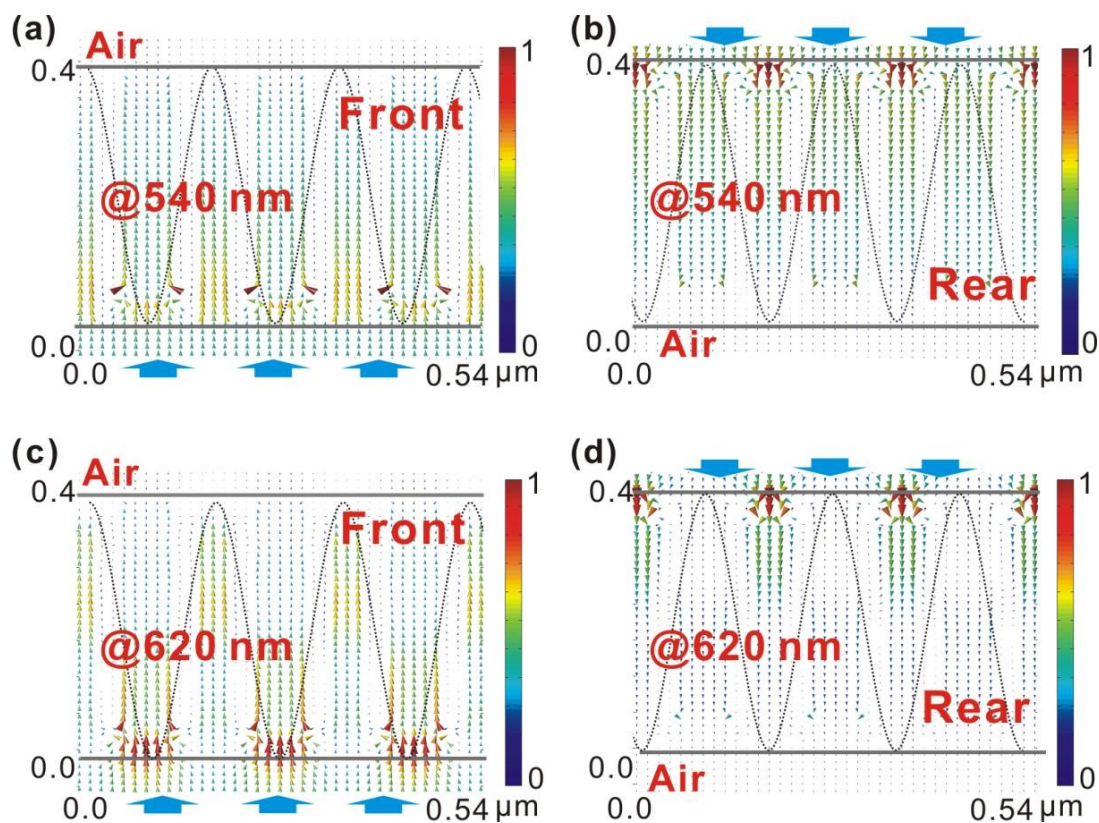


Fig. 6 Calculated Poynting vector \mathbf{S} (energy flow) distributions excited by a TM polarized plane for four scenarios at a wavelength of (a) 540 nm (front), (b) 540 nm (rear), (c) 620 nm (front) and (d) 620 nm (rear). Arrows denote the flow direction of the energy flow and a thicker and longer arrow indicates a stronger intensity of the photon flux. The black lines represent the interface of different dielectric.

To gain further insight into the origin of these unique optical modes, Poynting vector \mathbf{S} (energy flow) distributions for aforementioned four representative scenarios, which can clearly indicate how the light propagates in absorber before it is totally absorbed, were calculated with the excitation of a plane wave located at the semi-infinite air and PET for the front and the rear light incident, respectively. As

presented in Fig. 6a, b, localized CM enables the incident energy to form vortexes close to the interface between Au and Si₃N₄.⁴³ Meanwhile, the incident photons propagates along the nanocone toward the other interface induced by Rayleigh-Wood anomalies.⁴⁴ Besides, It is noteworthy that the partial photons crossing the gaps between the neighboring sidewalls near the incident plane indicate excitation of the localized SPM resonance.⁴⁵ As displayed in Fig. 6 c, d, similar to the scenario at 540 nm, localized CM and localized SPM effects confine majority of the incident photons around the interface between Au and Si₃N₄. Additionally, the fundamental TM mode guided in the areas close to the middle of the UV-nanonipples does not reach the cut-off frequency because the size of the nanonipple is much smaller than the incident wavelength, then the energy flow was squeezed into the air nanogroove and almost completely absorbed by the Au layer, thus resulting in Ohmic losses increase in the end.⁴⁶

4. Conclusions

In summary, we have demonstrated a simple and versatile method to fabricate a novel wide-band bidirectional visible light absorber based on quasi-periodic nanocone array coated with a dielectric-loaded mono-layer of gold. The proposed BLA are capable of absorbing light from the front surface and rear surface simultaneously, yielding measured average front absorption of 87.4% and the corresponding 76.2% rear absorbtivity respectively. Moreover, the bidirectional absorption property retains well with respect to the incident angle varying from 0° to 60°. The experimental and

theoretical evidences demonstrated above indicate that the unique bidirectional absorption properties are attributed to the combination of the localized CM, the localized SPM, GMR and the hybrid coupling between CM and SPM, leading to ultimately Ohmic losses increase within Au layer. This proposed structure and interesting bidirectional absorption properties features makes it an outstanding candidate for potential application in thermophotovoltaics, thermal emitters and other advanced optoelectronics.

Acknowledgments

This work was financially supported by the National Science Foundation (NSFC) (61575133, 51302179, 61505134); Key Natural Science Foundation of the Higher Education Institutions of Jiangsu Province (14KJB140014); Natural Science Foundation of Jiangsu Province (BK20140357); the Science and Technology Project of Suzhou (ZXG201427); Zhejiang Key Discipline of Instrument Science and technology; Project funded by the Priority Academic Program Development of Jiangsu Higher Education Institutions (PAPD).

Notes and references

- 1 N. I. Landy, S. Sajuyigbe, J. J. Mock, D. R. Smith, W. J. Padilla, *Phys. Rev. Lett.*, 2008, **100**, 207402.
- 2 X. Liu, T. Tyler, T. Starr, A. F. Starr, N. M. Jokerst, W. J. Padilla, *Phys. Rev. Lett.*, 2011, **107**, 045901.
- 3 A. Tittl, P. Mai, R. Taubert, D. Dregely, N. Liu, H. Giessen, *Nano Lett.*, 2011, **11**,

4366.

- 4 J. Qian, L. Jiang, F. Cai, D. Wang, S. He, *Biomaterials*, 2011, **32**, 1601.
- 5 W. Li, J. Valentine, *Nano Lett.*, 2014, **14**, 3510.
- 6 J. A. McLean, K. A. Stumpo, D. H. Russell, *J. Am. Chem. Soc.*, 2005, **127**, 5304.
- 7 A. M. Morales, C. M. Lieber, *Science*, 1998, **279**, 208.
- 8 C. Hu, L. Liu, Z. Zhao, X. N. Chen, X. Luo, *Opt. Express*, 2009, **17**, 16745.
- 9 Z. P. Yang, L. Ci, J. A. Bur, S. Y. Lin, P. M. Ajayan, *Nano Lett.*, 2008, **8**, 446.
- 10 Y. Cui, Y. He, Y. Jin, F. Ding, L. Yang, Y. Ye, S. M. Zhong, Y. Y. Lin, S. He, *Laser Photonics Rev.*, 2014, **8**, 495.
- 11 S. Shu, Z. Li, Y. Y. Li, *Opt. Express*, 2013, **21**, 25307.
- 12 M. A. Kats, R. Blanchard, P. Genevet, F. Capasso, *Nat. Mater.*, 2013, **12**, 20.
- 13 B. Zhang, Y. Zhao, Q. Hao, B. Kiraly, I. C. Khoo, S. Chen, T. J. Huang, *Opt. Express*, 2001, **19**, 15221.
- 14 A. Roszkiewicz, W. Nasalski, *Opt. Lett.*, 2012, **37**, 3759.
- 15 P. Feng, W. D. Li, W. Zhang, *Opt. Express*, 2015, **23**, 2328.
- 16 Y. F. Huang, S. Chattopadhyay, Y. J. Jen, C. Y. Peng, T. A. Liu, Y. K. Hsu, L. C. Chen, *Nat. Nanotechnol.*, 2007, **2**, 770.
- 17 J. Zhu, Z. Yu, G. F. Burkhard, C. M. Hsu, S. T. Connor, Y. Xu, Y. Cui, *Nano Lett.*, 2008, **9**, 279.
- 18 L. Hu, G. Chen, *Nano Lett.*, 2007, **7**, 3249.
- 19 T. Cao, C. W. Wei, R. E. Simpson, L. Zhang, M. J. Cryan, *Sci. Rep.*, 2014, **4**, 3955.
- 20 C. Argyropoulos, K. Q. Le, N. Mattiucci, G. D'Aguzzo, A. Alu, *Phys. Rev. B.*, 2013, **87**, 205112.

- 21 M. Bora, E. M. Behymer, D. A. Dehlinger, J. A. Britten, C. C. Larson, A. S. Chang, T. C. Bond, *Appl. Phys. Lett.*, 2013, **102**, 251105.
- 22 M. Yan, J. Dai, M. Qiu, *J. Opt.*, 2014, **6**, 025002.
- 23 J. Yang, X. Hu, X. Li, Z. Liu, Z. Liang, X. Jiang, J. Zi, *Phys. Rev. B.*, 2009, **80**, 125103.
- 24 E. E. Narimanov, A. V. Kildishev, *Appl. Phys. Lett.*, 2009, **95**, 041106.
- 25 T. Søndergaard, S. M. Novikov, T. Holmgaard, R. L. Eriksen, J. Beermann, Z. Han, S. I. Bozhevolnyi, *Nat. Comm.*, 2012, **3**, 969.
- 26 G. Tagliabue, H. Eghlidi, D. Poulikakos, *Nanoscale*, 2013, **5**, 9957.
- 27 M. K. Hedayati, M. Javaherirahim, B. Mozooni, R. Abdelaziz, A. Tavassolizadeh, V. S. K. Chakravadhanula, M. Elbahri, *Adv. Mater.*, 2011, **23**, 5410.
- 28 M. K. Hedayati, F. Faupel, M. Elbahri, *Appl. Phys. A.*, 2012, **109**, 769.
- 29 H. Masuda, K. Fukuda, *Science*, 1995, **268**, 1466.
- 30 C. W. Cheng, E. J. Sie, B. Liu, C. H. A. Huan, T. C. Sum, H. D. Sun, H. J. Fan, *Appl. Phys. Lett.*, 2010, **96**, 071107.
- 31 C. C. Lin, S. Y. Chen, S. Y. Cheng, H. Y. Lee, *Appl. Phys. Lett.*, 2004, **84**, 5040.
- 32 J. Zhang, S. Shen, X. X. Dong, L. S. Chen, *Opt. Express*, 2014, **22**, 1842.
- 33 L. Zhou, Q. D. Ou, Y. Q. Li, H. Y. Xiang, L. H. Xu, J. D. Chen, J. X. Tang, *Adv. Funct. Mater.*, 2015, **25**, 2660.
- 34 L. Zhou, X. X. Dong, G. C. Lv, J. Chen, S. Shen, *Opt. Commun.*, 2015, **342**, 167.
- 35 K. Aydin, V. E. Ferry, R. M. Briggs, H. A. Atwater, *Nat. Commun.*, 2011, **2**, 517.
- 36 F. Pardo, P. Bouchon, R. Hařlar, J. L. Pelouard, *Phys. Rev. Lett.*, 2011, **107**, 093902.
- 37 L. Fu, H. Schweizer, T. Weiss, H. Giessen, *JOSA B.*, 2009, **26**, B111.

- 38 A. Christ, T. Zentgraf, J. Kuhl, S. G. Tikhodeev, N. A. Gippius, H. Giessen, *Phys. Rev. B.*, 2004, **70**, 125113.
- 39 A. S. Vengurlekar, *Opt. Lett.*, 2008, **33**, 1669.
- 40 W. E. Sha, W. C. Choy, W. C. Chew, *Opt. Lett.*, 2011, **36**, 478.
- 41 H. T. Miyazaki, Y. Kurokawa, *Appl. Phys. Lett.*, 2006, **89**, 211126.
- 42 J. A. Porto, F. J. Garcia-Vidal, J. B. Pendry, *Phys. Rev. Lett.*, 1999, **83**, 2845.
- 43 S. Shen, W. Qiao, Y. Ye, Y. Zhou, L. S. Chen, *Opt. Express*, 2015, **23**, 963.
- 44 E. C. Kinzel, X. Xu, *Opt. Lett.*, 2010, **35**, 992.
- 45 N. J. Halas, S. Lal, W. S. Chang, S. Link, *Chem. Rev.*, 2011, **111**, 3913.
- 46 Y. Cui, K. H. Fung, J. Xu, H. Ma, Y. Jin, S. He, N. X. Fang, *Nano Lett.*, 2012, **12**, 1443.

The table of contents entry

A wide-band bidirectional visible light absorber based on quasi-periodic nanocone array coated with a dielectric-loaded mono-layer of gold.

ToC figure

